

Molecular Emission in Dense Massive Clumps from the Star-Forming Regions S231-S235

D. A. Ladeyschikov,¹ M. S. Kirsanova,² A. P. Tsvilev,³ and A. M. Sobolev¹

¹*Kourovka Astronomical Observatory, Ural Federal University, Ekaterinburg, 620000 Russia*

²*Institute of Astronomy of the Russian Academy of Sciences, Moscow, 119017 Russia*

³*Pushchino Radio Astronomy Observatory, Lebedev Physical Institute of the Russian Academy of Sciences, Pushchino, 142290 Russia*

The article deals with observations of star-forming regions S231-S235 in 'quasi-thermal' lines of ammonia (NH_3), cyanoacetylene (HC_3N) and maser lines of methanol (CH_3OH) and water vapor (H_2O). S231-S235 regions is situated in the giant molecular cloud G174+2.5. We selected all massive molecular clumps in G174+2.5 using archive CO data. For the each clump we determined mass, size and CO column density. After that we performed observations of these clumps. We report about first detections of NH_3 and HC_3N lines toward the molecular clumps WB89 673 and WB89 668. This means that high-density gas is present there. Physical parameters of molecular gas in the clumps were estimated using the data on ammonia emission. We found that the gas temperature and the hydrogen number density are in the ranges 16-30 K and $2.8\text{-}7.2 \times 10^3 \text{ cm}^{-3}$, respectively. The shock-tracing line of CH_3OH molecule at 36.2 GHz is newly detected toward WB89 673.

1. INTRODUCTION

One of the most topical and rapidly developing fields in astrophysics is the study of star-forming regions. A great number of molecules in the interstellar medium which are quite intensively radiating in radio lines gives a plenty of possibilities for this. It is considered currently that star formation occurs in regions of high concentration of molecular gas, clumps, the main component of which is molecular hydrogen (H_2). As hydrogen molecules in clumps do not radiate in the radio range, radio lines of other molecules are used to trace the presence of molecular gas, ongoing processes, and conditions in the interstellar medium. Particularly, molecular lines of carbon monoxide (CO) show general distribution of molecular gas in the star-forming regions of our Galaxy [1]. Lines of ammonia (NH_3) molecule are tracers of temperature [2] and gas high density [3]. Molecular lines of cyanoacetylene (HC_3N) are also gas high density tracers [4]. The observed data shows that maser and "quasi-thermal" lines of methanol (CH_3OH) make it possible to investigate outflows from young stellar objects and shock waves in the interstellar medium [5–9], and masers at the transition of water molecule (H_2O) indicate ongoing active star-forming processes [10]. On the whole, the present information provides an opportunity of a comprehensive study of star-forming regions including estimation of their physical parameters as well.

The goal of this paper is to study massive molecular clumps of the star-forming regions S231–S235 situated in the giant molecular cloud (GMC) G174+2.5. In this direction, there are four advanced regions of ionized hydrogen: S231, S232, S233, and S235 in accordance with the catalog by Sharpless [11]. Researchers distinguish

six well-studied young star clusters: S235 Central, S235 East 1, S235 East 2, and S235 AB (see, e.g., [12–14]), S233 IR (see [15–17]), and G173.57+2.43 (see [18, 19]). Cross-identification of clusters called differently by various authors is given in the paper by Camargo [20]. On the periphery, there are the less-studied star-forming regions WB89 673 and WB89 668 which are named from the Wouterloot–Brand catalog [21]. Previously Heyer et al. [22] studied the morphology and kinematics of this star-forming complex from the CO radio lines. The maps of CO line emission show that the most prominent star-forming regions in the cloud G174+2.5 are S231–S235. Distance estimates to them range from 1.5 to 2.3 kpc [23, 24]. The regions S231–S235 are situated in the direction close to the galactic anticenter. As follows from the paper by Dame et al. [25], no such star-forming regions more distant from the Sun are observed in this direction in the Galaxy.

In the present paper, we present the results of observations of molecular radio lines in molecular clumps, previously selected using the archive data on the CO line emission in the giant molecular cloud G174+2.5, which have been carried out at the radio telescope RT-22 of the Pushchino Radio Astronomy Observatory of the Lebedev Physical Institute of the Russian Academy of Sciences (PRAO ASC LPI). First, we searched for class I methanol masers in the direction to the selected molecular clumps. After detection of them, to prove the presence of dense gas and to determine physical parameters of gas in the clumps, density and temperature first of all, we conducted observations in the NH_3 and HC_3N lines. Thus, in this paper we present general characteristics of emission of molecules toward the star-forming regions S231–S235 and estimations of the physical parameters of the gas and of the mass of molecular clumps. Instruments, sources, and methods we used

are described in the corresponding Sections.

2. SELECTION OF THE OBJECTS FOR OBSERVATION

We used the archive data with observations in the $^{12}\text{CO}(1-0)$ and $^{13}\text{CO}(1-0)$ lines in order to select molecular clumps toward the star-forming regions S231–S235 to estimate their physical characteristics. They are described in Section 3. The details of method of physical parameters’ calculation are given in Annex A. We overlaid the positions of the IRAS sources onto the derived map of column density of ^{13}CO toward the star-forming regions S231–S235 and limited the research area with a circle of a radius of $50'$ around the center of ionized hydrogen S231 ($\alpha_{\text{J2000}} = 5^{\text{h}}39^{\text{m}}45^{\text{s}}$, $\delta_{\text{J2000}} = 35^{\circ}54'02''$) (see Fig. 1).

For observations in the NH_3 line, we selected the positions of centers of the ^{13}CO column density peaks. In the CH_3OH and HC_3N lines, the sources were observed at the positions which coincide or are quite close to local peaks of ^{13}CO column density. In the case of close proximity of several IRAS sources to the peak, if the angular distance between them was smaller than the beam size of the RT-22, then we chose the source closest to the ^{13}CO peak as a pointing source. As a result of this analysis, we visually selected 10 molecular clumps to observe at the RT-22. We added a calibration source Dr21 to our sample for comparing the observed results with other works.

Table 1 shows the coordinates and general physical characteristics of the sources. Radial velocity and clump sizes are derived from the data on emission in the $^{13}\text{CO}(1-0)$ line. Excitation temperature is calculated using the data on emission in the $^{12}\text{CO}(1-0)$ line, its average value is shown within the limits of molecular clump sizes. Numerical values of column density are calculated on the basis of the map of its distribution presented in Fig 1. The table shows average column densities of H_2 and masses within the limits of molecular clump sizes. The last column gives virial parameter $\alpha_{\text{vir}} \equiv M_{\text{vir}}/M$ (see the description in Section 5.1).

All the selected molecular clumps radiate in the continuum at a wavelength of 1.12 mm from the Bolocam [26] survey data which is indicative of heated dense gas in them. Almost all of them correspond to young star clusters according to the data from infrared sky surveys Wide-Field Infrared Survey Explorer (WISE, [27]) and UKIRT Infrared Deep Sky Survey (UKIDSS, [28]). Section 6.2 in detail considers the association of clumps and clusters.

3. ARCHIVE DATA ON THE CO EMISSION

Data on emission in the $^{12}\text{CO}(1-0)$ and $^{13}\text{CO}(1-0)$ lines are obtained using the results of observations within the program of highly-accurate survey of the Galactic plane in the line of the CO molecule [29] conducted at the 13.7-m telescope of the Five College Radio Astronomy Observatory (FCRAO) with the Second Quabbin Observatory Imaging Array (SEQUOIA), a 32-pixel focal receiver. The regions S231–S235 were mapped in January of 2000. The map of line emission of both CO isotopes covers the region with a size of $150' \times 150'$ with the center at $l = 173^{\circ}25$, $b = 2^{\circ}75$ ($\alpha_{\text{J2000}} = 5^{\text{h}}40^{\text{m}}$, $\delta_{\text{J2000}} = 36^{\circ}07'$). The beam size for this telescope is $45''$ for $^{12}\text{CO}(1-0)$ and $47''$ for $^{13}\text{CO}(1-0)$. Observed frequency was set 115.27120 GHz for the $^{12}\text{CO}(1-0)$ line and 110.20135 GHz for $^{13}\text{CO}(1-0)$. Spatial step was $22''.5$ which is two times smaller than the half-power beamwidth (HPBW). Velocity step was equal to 0.127 km s^{-1} for $^{12}\text{CO}(1-0)$ and 0.133 km s^{-1} for $^{13}\text{CO}(1-0)$. The noise level $\sigma_{T_{\text{mb}}}$ for $^{12}\text{CO}(1-0)$ was 1.1 K and for $^{13}\text{CO}(1-0)$ —0.63 K on main-beam temperature scale. For the reduction of data in the CO lines and the calculation of physical parameters, we used the MIRIAD package [30]. Integrating and statistical analysis of physical parameters were carried out with the package ds9 [31].

4. OBSERVED DATA

All the observed data in the present work have been obtained at the radio telescope RT-22 of the Puschino Radio Astronomy Observatory (PRAO ASC LPI). We conducted several observational sessions in 2013, 2014, and 2015 using scans of 4–7 min. Data from each scan were calibrated to antenna temperature by the reference signal from the noise generator with a known antenna temperature and were corrected for atmospheric absorption. Next we obtained spectra averaged over days, then averaged between days. The antenna temperature T_{a} was reduced to the main beam brightness temperature T_{mb} using the main beam efficiency η_{mb} . Figures 2, 3, and 4 show the spectra of the obtained lines on T_{mb} scale, and Tables 2, 3, and 4 present their observed parameters. To estimate the quality of the obtained data, we observed the source Dr21 and compared the observations with those presented in [32–34]. Calibration accuracy from the result of comparison is about 10–30%.

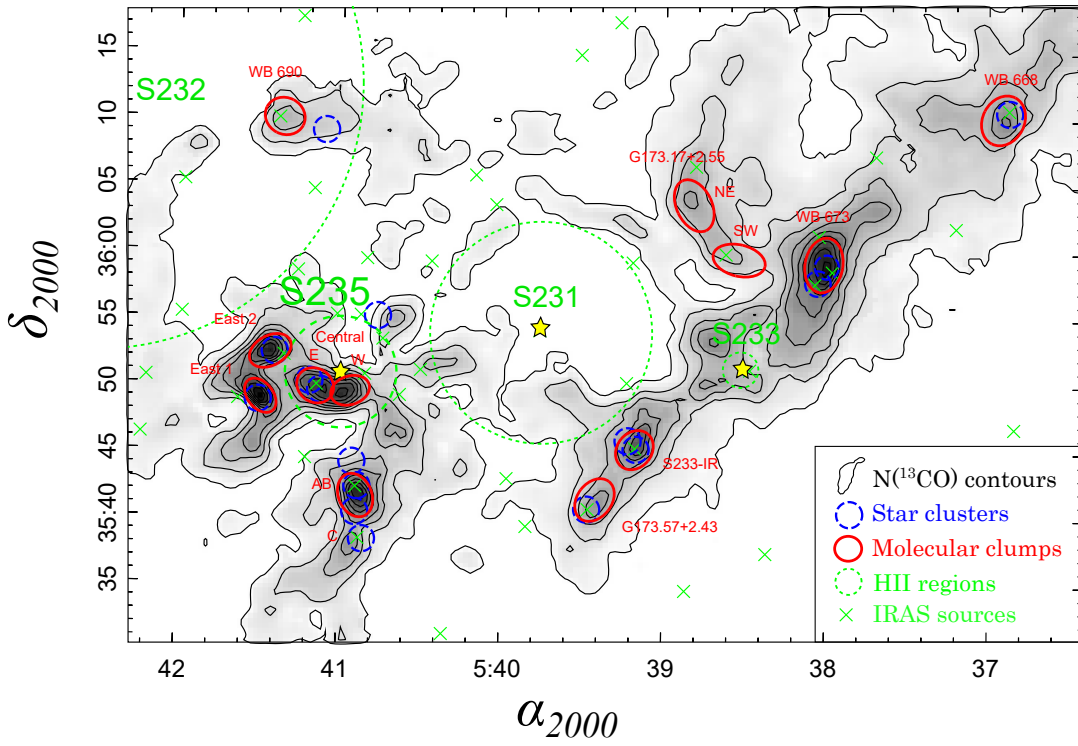


Figure 1. Distribution of column density of ^{13}CO toward the star-forming region S231–S235. Outer contour corresponds to the value $5 \times 10^{15} \text{ cm}^{-2}$, the most inner— $6 \times 10^{16} \text{ cm}^{-2}$, contour step is $8.4 \times 10^{15} \text{ cm}^{-2}$. Crosses denote the positions of the IRAS sources. Red ellipses mark molecular clumps selected within the frame of the present paper for observations in the lines of methanol, cyanoacetylene, and ammonia. The sizes of ellipses correspond to the sizes of molecular clumps. Blue dashed circles denote the positions of young star clusters from the data by Camargo et al. [20]. Green dashed circles mark the regions of ionized hydrogen (H II). The radii of the circles correspond to the radii of the H II regions from the DSS R images. Star-shaped figures show the position of stars ionizing the H II regions.

Table 1. Catalog of molecular clumps in the ^{13}CO line with general physical parameters (see the text for details).

Name	α_{J2000} , h m s	δ_{J2000} , ° ' "	θ_{FWHM} , '	R , pc	V_{LSR} , km s^{-1}	ΔV , km s^{-1}	T_{ex} , K	$N(\text{H}_2)$, 10^{22} cm^{-2}	$M(\text{H}_2)$, M_{\odot}	$\tau(^{13}\text{CO})$	α_{vir}
WB89 690	5 41 21.6	+36 10 00	3.1×2.7	0.87	−21.0	1.83	16.5	1.45	733	0.65	0.86
WB89 668	5 36 54.3	+36 10 16	3.9×3.1	1.06	−17.2	2.70	14.1	1.60	1199	0.85	1.40
WB89 673	5 38 00.6	+35 59 17	4.1×2.8	1.04	−19.5	3.16	20.8	2.90	2112	0.74	1.07
G173.17+2.55 NE	5 38 49.0	+36 03 41	4.1×2.6	0.99	−17.9	2.44	16.4	1.66	1095	0.69	1.18
G173.57+2.43	5 39 24.7	+35 41 28	3.5×2.6	0.90	−16.8	2.38	17.2	1.70	932	0.65	1.20
S233-IR	5 39 10.2	+35 45 15	3.1×2.6	0.83	−16.9	2.76	22.1	2.29	1048	0.55	1.31
S235 Central E	5 41 08.8	+35 49 47	2.9×2.5	0.83	−19.6	1.92	35.6	3.67	1683	0.35	0.39
S235 Central W	5 40 55.8	+35 49 27	3.0×2.1	0.74	−21.5	1.93	31.6	3.65	1347	0.49	0.45
S235 East1	5 41 29.0	+35 48 58	2.9×1.9	0.74	−18.9	1.80	32.7	4.31	1591	0.51	0.33
S235 East2	5 41 25.6	+35 52 21	3.4×2.2	0.87	−20.8	1.78	29.4	3.62	1822	0.55	0.33
S235-AB	5 40 53.3	+35 41 35	3.4×2.5	0.90	−16.5	2.30	27.0	3.53	1935	0.59	0.54

4.1. Observations at the 8 mm wavelength

To execute the program of observations, we used a two-channel radiometer of RT-22 of 8 mm wavelength. It is designed for simultaneous observations of two spectral lines in case the line frequencies are in the range of 34 to 38 GHz and the difference between the line frequencies is not greater than 2 GHz. Within the present work, the obser-

vations were carried out in the methanol line (4_{-1-3_0} E , 36.1 GHz) and cyanoacetylene line ($J = 4-3$, 36.3 GHz) using the spectrum analyser with a constant bandwidth of 50 MHz. Spectral resolution was 24.41 kHz which corresponds to 0.20 km s^{-1} for the methanol line frequency. Rest frequency for the CH_3OH line was set 36169.29 MHz and for the HC_3N line—36392.33 MHz. We used the ON-ON method of observations based on diagram modula-

tion [35], with which we obtain a double signal as a result. Separation between beams (horns) was $23'$. The half-power beam width (HPBW) was $2'$, the beam efficiency $\eta_{\text{mb}} = 0.32$. The system temperature T_{sys} at the time of observations was within the range of 200 to 240 K. With average integration time for each source from 2 to 3 hours per every day of observations, the total integration time was from 5 to 8 hours for sources with the detected line and from 1 to 2 hours for sources without the detected line. The achieved noise level $\sigma_{T_{\text{mb}}}$ is in the range of 0.05 to 0.28 K on brightness temperature scale. We checked the observed radial velocity using the source Dr21 ($\alpha_{\text{J2000}} = 20^{\text{h}}38^{\text{m}}55^{\text{s}}$, $\delta_{\text{J2000}} = 42^{\circ}19'23''$) which has the methanol line at 36.1 GHz detected earlier in the paper by Liechti et al. [36] and the cyanoacetylene line—in the the paper by Tolmachev et al. [32]. The results of this checking showed that the derived radial velocities of the methanol line ($V_{\text{CH}_3\text{OH}} = -2.73 \pm 0.01 \text{ km s}^{-1}$) and cyanoacetylene line ($V_{\text{HC}_3\text{N}} = -3.08 \pm 0.06 \text{ km s}^{-1}$) in the Dr21 source are within the error margin in accordance with [32, 36].

The program CLASS from the package GILDAS [37] were used for data reduction. The shape of the line profiles in methanol and cyanoacetylene spectra was approximated with the standard GAUSS method. Owing to a complex structure of the methanol line, two Gaussian functions were used in approximation.

4.2. Observations at the 13 mm wavelength

Observations in the ammonia line (NH_3 (1,1) and (2,2), 23.6 GHz) were carried out on the single-channel radiometer of 13.5 mm wavelength. For the transition (1,1), we used a rest frequency of 23694.495 MHz and for the line (2,2)—23722.633 MHz. We used the ON-ON method based on diagram modulation [35], with a double signal as a result. Separation between beams (horns) was $10'$. The half-power beamwidth (HPBW) was $2'6$ and the beam efficiency factor $\eta_{\text{mb}} = 0.38$. Two sessions of observations were conducted, in 2013 and 2015. System temperature during the observations was in the range of 110 to 190 K on the antenna temperature scale.

In 2013, only the NH_3 (1,1) line was observed for initial detection of ammonia emission in the selected sources. We used the band of the spectrum analyzer with a width of 12.5 MHz and 2048 channels. Spectral resolution was about 6.1 kHz which corresponds to approximately 0.08 km s^{-1} for the rest frequency of the ammonia line. Integration time for the sources was 1–2 hours, the achieved noise level $\sigma_{T_{\text{mb}}}$ was in the range of 0.1 to 0.2 K for different sources on the brightness temperature scale.

In 2015, we simultaneously observed two low-level ammonia lines in noise transitions (1,1) and (2,2) for estimating the physical parameters of gas. We used an analyzer band of 50 MHz, thus the spectral resolution was about 24.4 kHz corresponding to approximately 0.31 km s^{-1} for the rest frequency of the ammonia line. Central frequency of the band of the spectrum analyzer was set in the middle between transitions (1,1) and (2,2) so that both transitions fall within the analyzer band. The distance between frequencies of two transitions of the NH_3 line was 28.138 MHz which was enough for their simultaneous detection with the spectrum analyzer with a band width of 50 MHz. Integration time for the sources with the detected line was 9–15 hours and for the sources without the detected line—2–5 hours. The achieved level $\sigma_{T_{\text{mb}}}$ for the sources with detection was from 0.01 to 0.04 K.

We approximated the spectra of the ammonia lines using the NH_3 (1,1) method from the CLASS package [37], and the SMOOTH procedure from the same package was used for further smoothing.

5. RESULTS

5.1. Masses of Clumps and Amount of Molecular Hydrogen in them

Determining column density and gas mass in the studied molecular clumps, at large we followed the method described in the paper by Roman-Duval et al. [38] with some changes. Formulas for determination of physical parameters of the clumps are given in Annex A. The estimation was made in the approximation of local thermodynamic equilibrium (LTE). To estimate the excitation temperature, we have used the data on emission in the ^{12}CO molecule line, as it is optically thick which is proved by the low ratio of intensities of lines $I(^{12}\text{CO})/I(^{13}\text{CO}) \approx 3\text{--}6$ as compared to the ratio of molecule abundances $^{12}\text{CO}/^{13}\text{CO} \approx 50\text{--}70$. To estimate the column density of the H_2 molecules, we used the emission in the ^{13}CO line which is optically thinner than the ^{12}CO line.

To estimate the mass, we used a number of constants. The ratio of abundances $\text{CO}/\text{H}_2 = 8 \times 10^{-5}$ is in accordance to Simon [39]. The distance to all the clumps is assumed equal to $2.1 \pm 0.5 \text{ kpc}$ which is the average of the estimated distances to young star cluster from the G174+2.5 GMC from the paper by Camargo et al. [20]. For the present distance, the average galactocentric radius is 10.1 kpc, or $1.26D_{\odot}$ using the estimation of distance from the Sun to the Galactic center $D_{\odot} = 8.0 \text{ kpc}$ from the paper by Reid et al. [40]. With reference to the paper by Langer and Penzias [41], the ratio

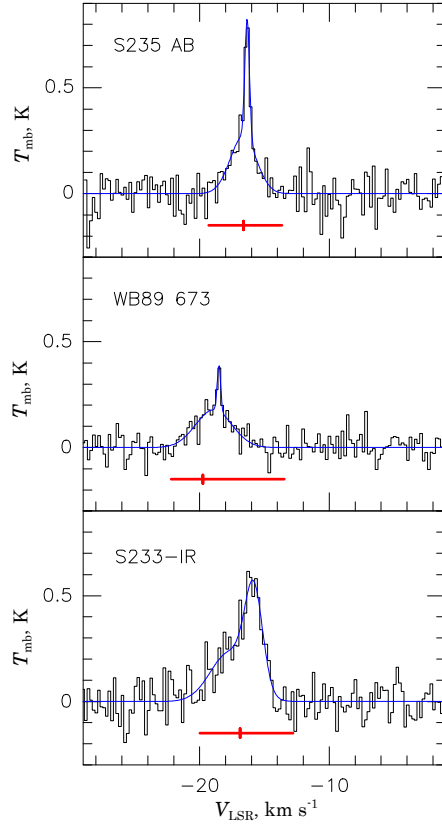


Figure 2. Spectra of the detected sources in the CH₃OH line at a frequency of 36.2 GHz. A blue line denotes approximation of line profiles with the Gaussian function, a red line segment at the lower part of spectra shows the velocity range of ¹³CO, and the peak of the ¹³CO line is marked with a tick.

Table 2. Parameters of the methanol lines (CH₃OH) at 36.2 GHz. An asterisk denotes the sources in which the line was detected for the first time. In each detected source two components of emission are presented, the narrow and wide (see the discussion on this in Section 6.3). The positions of the associated IRAS sources were chosen as the coordinates for the sources, t —integration time, and 1σ —achieved noise level. Estimation errors are given in brackets.

Source	IRAS	T_{mb} , K	V , km s ⁻¹	ΔV , km s ⁻¹	t , min.	1σ , K
WB89 690	05380+3608	<0.08			346	0.08
WB89 668	05335+3609	<0.10			173	0.10
WB89 673*	05345+3556	0.21 (0.04)	-18.51 (0.05)	0.3 (0.10)	500	0.05
		0.17 (0.04)	-18.91 (0.16)	3.2 (0.38)	500	0.05
S233-IR	05358+3543	0.47 (0.07)	-15.81 (0.09)	1.6 (0.2)	386	0.08
		0.23 (0.07)	-17.7 (0.48)	3.5 (0.8)	386	0.08
G173.57+2.43	05361+3539	< 0.28			180	0.28
S235-AB	05375+3540	0.57 (0.04)	-16.34 (0.03)	0.42 (0.07)	353	0.07
		0.27 (0.04)	-16.64 (0.15)	2.38 (0.34)	353	0.07
S235 Central E	05377+3548	<0.15			126	0.15
S235 East1	05382+3547	<0.13			106	0.13
S235 East2	05379+3550	<0.13			113	0.13
Dr21	-	1.82 (0.06)	-2.73 (0.02)	0.49 (0.04)	333	0.09

of abundances ¹²C/¹³C at such galactocentric distance is about 70, thus, the ratio of abundances $^{13}\text{CO}/\text{H}_2 = [\text{CO}/\text{H}_2]/[^{12}\text{C}/^{13}\text{C}] \simeq 1.14 \times 10^{-6}$.

This value was used to calculate the H₂ column density and clump masses.

We used the GaussClump algorithm [42] to de-

tect the molecular clumps more accurately in the ¹³CO line. This algorithm works on the principle of fitting of three-dimensional Gaussians into the observed data cube “position–position–radial velocity” (PPV) starting from global emission maximum. As a threshold for minimum spatial size of clumps

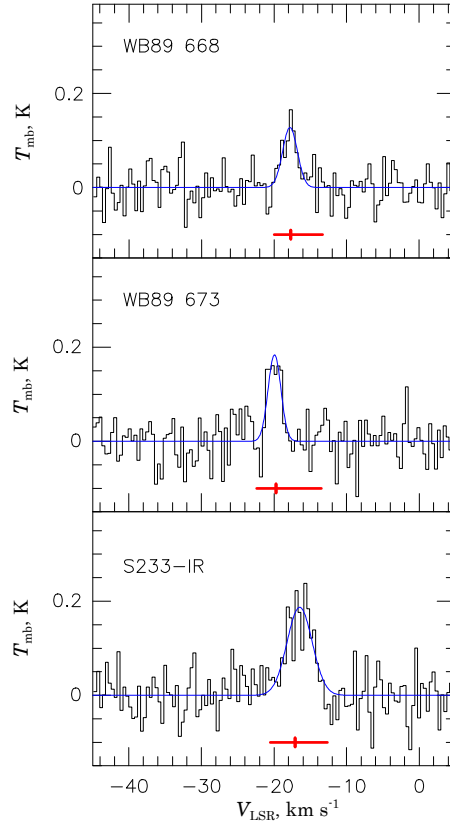


Figure 3. Spectra of the sources detected in the HC_3N line at 36.4 GHz. The same legend as for Fig. 2.

Table 3. Parameters of the cyanoacetylene lines (HC_3N) at 36.4 GHz. An asterisk denote the sources in which the line was detected for the first time. The positions of the associated IRAS sources were chosen as the coordinates for the sources, t —integration time, and 1σ —achieved noise level. Estimation errors are given in brackets.

Source	IRAS	T_{mb} , K	V , km s^{-1}	ΔV , km s^{-1}	t , min.	1σ , K
WB89 690	05380+3608	< 0.09			346	0.09
WB89 668*	05335+3609	0.12 (0.03)	-17.80 (0.20)	2.4 (0.5)	460	0.06
WB89 673*	05345+3556	0.18 (0.04)	-19.94 (0.14)	2.0 (0.26)	293	0.07
S233-IR	05358+3543	0.19 (0.07)	-16.4 (0.24)	4.1 (0.5)	353	0.05
G173.57+2.43	05361+3539	< 0.19			180	0.19
S235-AB	05375+3540	< 0.08			266	0.08
S235 Central E	05377+3548	< 0.14			126	0.14
S235 East1	05382+3547	< 0.12			106	0.12
S235 East2	05379+3550	< 0.17			113	0.17
Dr21	-	0.56 (0.06)	-3.08 (0.06)	2.9 (0.16)	343	0.06

(θ_{FWHM}), we set a value of $1'.7$, because at lower threshold, big molecular clumps are divided into individual components. However, even with such a threshold, some clumps (particularly, S235 Central and G173.17+2.55) divide into separate components which will be discussed further. Minimum line-width threshold (ΔV) for clumps is 0.8 km s^{-1} which is determined by the requirement of extraction of only massive clumps with relatively high dispersion of radial velocity. As a result of using the algorithm, we selected 12 clumps corresponding to the IRAS

sources by the criterion described in Section 2. Two clumps divide into individual components; they are S235 Central and G173.17+2.55, on which we will write in the discussion of results. The sizes of clumps are determined as full width at half maximum level (θ_{FWHM}). The mass of clumps is estimated after integrating the clump emission by the area corresponding to the size of clumps at half-intensity level. Table 1 shows the results of estimation of clump sizes, column density of H_2 , and mass. Figure 1 presents the map of distribution of column density of H_2 with

the overlaid sizes of molecular clumps.

Virial parameter of clumps $\alpha_{\text{vir}} \equiv M_{\text{vir}}/M_{\text{CO}}$ and radius R were calculated according to the definition in the paper by Kauffmann et al. [43], the formulas for calculation are given in Annex A. The distance to all the clumps was assumed equal to 2.1 kpc and the velocity dispersion was calculated from the ^{13}CO line width with the formula $\sigma_v = 2.35\Delta V_{13}$. Table 1 presents the derived α_{vir} and R values. It should be noted that determination methods for the clump radius R and angular size θ_{FWHM} presented in Table 1 differ: the first is determined from the clump area with the formula $R = \sqrt{A/\pi}$, the latter—from the width (FWHM) of the Gaussian function fitted in the clump intensity profile.

We determined that average column density of the ^{13}CO molecule toward the considered molecular clumps of the S231–S235 regions are within the range of $1.6 \times 10^{16} \text{ cm}^{-2}$ in WB 690 to $4.8 \times 10^{16} \text{ cm}^{-2}$ in S235 East 1. Using the above relation $^{13}\text{CO}/\text{H}_2 = 1.14 \times 10^{-6}$, one can obtain average column density of molecular hydrogen toward the clumps, from $1.45 \times 10^{22} \text{ cm}^{-2}$ in WB 690 to $4.21 \times 10^{22} \text{ cm}^{-2}$ in S235 East 1. The derived values should be regarded as a lower estimate of column density of molecular hydrogen, as the analysis of the CO line emission within the LTE tends to underestimate actual column densities by a factor of 1.3 to 7 in accordance to the paper by Padoan [44]. The mass of clumps from the CO data is within the range of $733 M_{\odot}$ in WB89 690 to $2112 M_{\odot}$ in WB89 673. The virial parameter α_{vir} varies from 0.33 in S235 East 2 to 1.31 in S233-IR. Its average value is $\overline{\alpha_{\text{vir}}} = 0.82$ which at large is indicative of correspondence of virial mass and mass from the ^{13}CO data.

The excitation temperature derived from the ^{12}CO data should be interpreted as the temperature of gas near the molecular cloud surface, as the ^{12}CO line is optically thick. According to the derived data (see Table 1), the molecular clump WB89 668 (14.1 K) has the “coldest” surface and the clump S235 Central E (35.6 K)—the “warmest” one. The average surface temperature of the molecular clumps is 24 K.

5.2. Lines-Tracers of Dense Molecular Gas

In the 36.2 GHz observations, the methanol lines were detected toward the molecular clumps WB89 673, S233-IR, and S235-AB. In the clump WB89 673, the methanol emission was detected for the first time. In most cases, the line profile shape differs from the Gaussian; and toward S233-IR, the line has an asymmetric structure with a pronounced blue wing. Two emission components, narrow and wide, can be distinguished in the detected methanol

lines. The width of narrow components is within the range of 0.3 to 1.6 km s^{-1} , for wide components—from 2.4 to 3.5 km s^{-1} . The positions of the narrow and wide components are shifted relative to each other by a value of 0.3 to 1.8 km s^{-1} . The difference between radial velocities of methanol and ^{13}CO lines does not exceed 1.2 km s^{-1} .

In the cyanoacetylene molecular line, we detected the emission toward the molecular clumps WB89 668, WB89 673, S233-IR, and S235 Central. The line HC_3N in the clumps WB89 668 and WB89 673 was detected for the first time. The line profile shapes are close to Gaussian, the average line width is about 2.4 km s^{-1} , except for S233-IR, the line width of which is $4.0 \pm 0.5 \text{ km s}^{-1}$. The difference between radial velocities of the HC_3N and CO lines does not exceed 0.5 km s^{-1} in the clumps WB89 668 and WB89 673. In the clump S233-IR, the HC_3N radial velocities are redshifted as compared to the ^{13}CO radial velocity. The difference between radial velocities is 1.4 km s^{-1} .

The ammonia emission was detected toward the molecular clumps WB89 668, WB89 673, G173.57+2.43, S233-IR, S235 Central, S235 East 1, S235 East 2, and S235-AB, for WB89 668 and WB89 673—for the first time. Hyperfine structure of the ammonia lines is detected with an accuracy needed to determine physical conditions in the molecular gas. The difference between radial velocities of the $\text{NH}_3(1,1)$ and ^{13}CO lines does not exceed 0.5 km s^{-1} in the clumps WB89 668, WB89 673, G173.57+2.43, S235-AB, and S233-IR.

Tables 2–4 show the parameters of the detected molecular lines.

5.3. Temperature and Density of Molecular Gas

To estimate the temperature and density of gas on the assumption of the local thermodynamic equilibrium (LTE), we used the ratio of the antenna temperature of the NH_3 spectrum main component to the antenna temperature of the satellite components of the hyperfine structure of the spectrum and the ratio between the main components of the transitions $\text{NH}_3(J, H) = (1,1)$ and $(2,2)$. The method of determination of physical parameters is described in Annex B. As a result, we derived estimations of the ammonia column density (N_{NH_3}), kinetic temperature (T_{kin}), and number density of molecular gas (n_{H_2}).

For the reason that the source size in the NH_3 line in the present complex (about 50–110'', see Table 6 from Kirsanova et al. [13]) is smaller than the RT-22 beam size (156''), then it is necessary to apply a correction for filling of the beam. We used the following formula (see equations 8.21–8.22 from

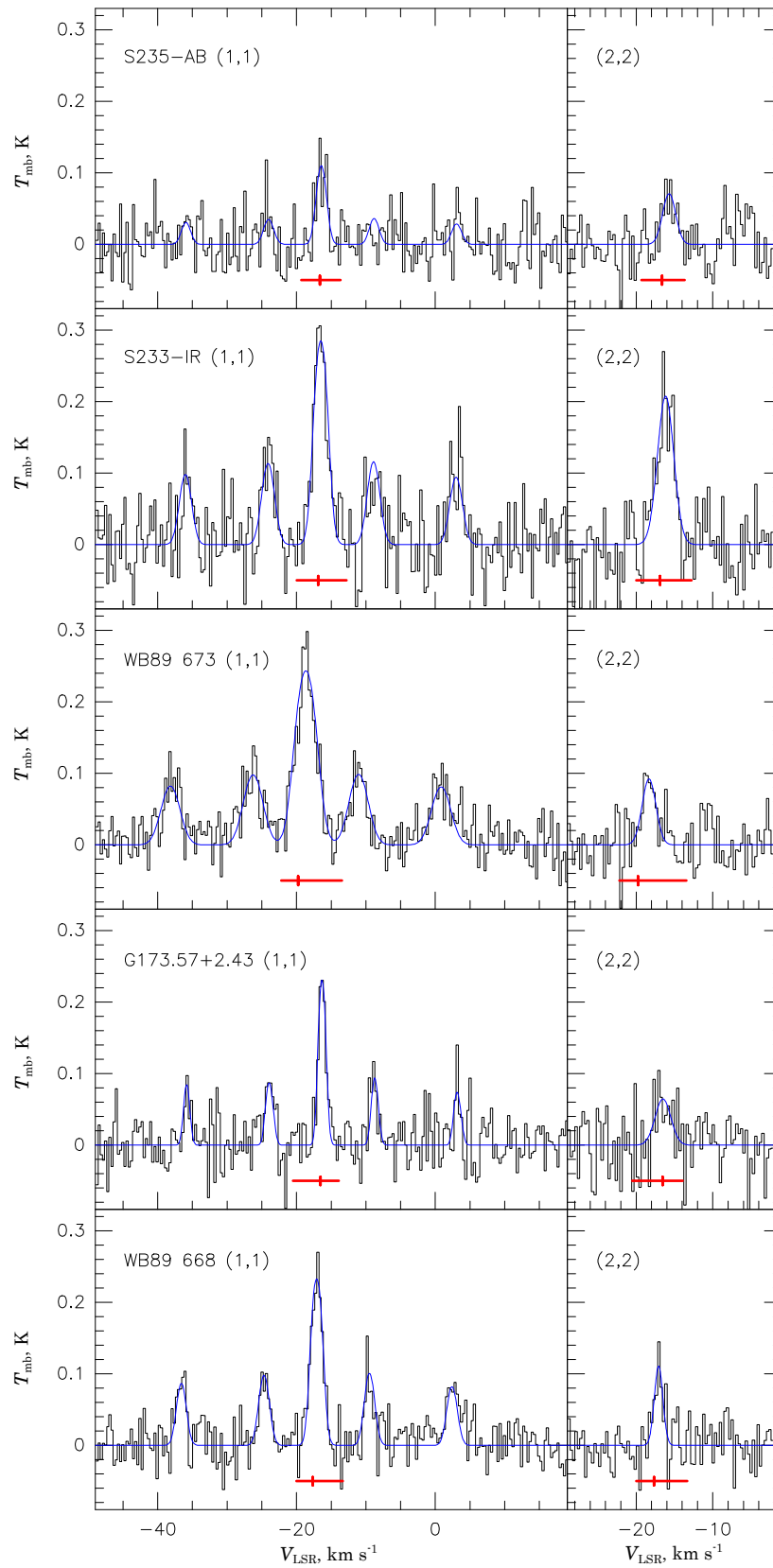


Figure 4. Spectra of the detected sources in the NH_3 line at 23.7 GHz. The same legend as for Fig. 2.

Table 4. Results of observations of star-forming regions in the ammonia line (NH_3) at a frequency of 23.7 GHz and physical parameters of gas in the molecular clumps (estimation errors are in brackets). An asterisk marks the sources, in which the line was detected for the first time. The positions of the ^{13}CO emission peak were chosen as the coordinates for the sources (see the coordinates from Table 1).

Source	(J, K)	T_{mb} , K	T_{B} , K	V , km s^{-1}	ΔV , km s^{-1}	$\tau_{(1,1)\text{m}}$	$\frac{\Theta_{\text{beam}}^2}{\Theta_{\text{maj}}\Theta_{\text{min}}}$	T_{kin} , K	$N(\text{NH}_3)$, 10^{14} cm^{-2}	$n(\text{H}_2)$, 10^3 cm^{-3}
(1)	(2)	(3)	(4)	(5)	(6)	(7)	(8)	(9)	(10)	(11)
WB89 668*	(1,1)	0.24 (0.01)	1.3 (0.1)	-17.1 (0.1)	1.7 (0.1)	1.4 (0.3)	4.3	16.5 (1.9)	7.3 (1.5)	4.2
	(2,2)	0.09 (0.01)	0.5 (0.1)	-17.1 (0.1)	1.5 (0.3)					
WB89 673*	(1,1)	0.25 (0.01)	1.1 (0.1)	-18.6 (0.1)	3.1 (0.1)	1.2 (0.3)	3.5	15.9 (1.5)	12.4 (2.2)	4.1
	(2,2)	0.08 (0.01)	0.4 (0.1)	-18.2 (0.2)	2.9 (0.6)					
S233-IR	(1,1)	0.28 (0.03)	2.2 (0.2)	-16.5 (0.1)	2.0 (0.1)	1.2 (0.4)	6.9	29.4 (11.8)	9.9 (1.9)	7.2
	(2,2)	0.21 (0.04)	1.7 (0.3)	-16.2 (0.1)	2.6 (0.3)					
G173.57+2.43	(1,1)	0.23 (0.03)	1.4 (0.2)	-16.3 (0.1)	1.2 (0.1)	1.2 (0.5)	5.1	14.4 (5.2)	5.1 (1.0)	5.6
	(2,2)	0.06 (0.01)	0.4 (0.1)	-16.5 (0.3)	2.3 (0.5)					
S235-AB	(1,1)	0.11 (0.03)	0.6 (0.2)	-16.4 (0.1)	1.6 (0.3)	0.6 (0.9)	4.4	27.4 (59.7)	2.2 (1.7)	2.8
	(2,2)	0.07 (0.04)	0.4 (0.21)	-15.7 (0.3)	2.1 (0.6)					

Rohlfs and Wilson [45]) to estimate the brightness temperature of a source:

$$T_{\text{B}} = T_{\text{mb}} \times \left(1 + \frac{\theta_{\text{beam}}^2}{\theta_{\text{maj}}\theta_{\text{min}}} \right) \quad (1)$$

where $T_{\text{mb}} = T_{\text{a}}/\eta_{\text{mb}}$ —the main-beam brightness temperature, $\theta_{\text{beam}} = 152''$ —the size of the RT-22 beam at a wavelength of 1.35 mm, θ_{maj} and θ_{min} —the sizes of sources (FWHM) along major and minor axes.

In order to estimate sizes of sources in the NH_3 line, we used the data on emission in the continuum at a wavelength of 1.1 mm from the Bolocam survey [26]. The comparison of emission sources in the continuum at a wavelength of 1.1 mm and in the NH_3 line toward S235 Central, East 1, East 2 [13], S233-IR [46], and G173.57+2.43 [47] showed that their sizes correspond to each other, thus, for brightness temperature estimation in the NH_3 line, one can use source sizes at a wavelength of 1.1 mm. The source sizes were determined with fitting of two-dimensional Gaussians into images by the IMFIT method from the MIRIAD package [30]. The determination results are presented in Table 5. For calculating the physical parameters of gas from the NH_3 lines, we used brightness temperatures obtained from formula (1).

Table 4 shows the derived physical parameters. Table legend: T_{mb} —main-beam brightness temperature, T_{B} —brightness temperature of a source, $\tau_{(1,1)\text{m}}$ —optical depth of the main component of the (1,1) line. Column 8 gives a coefficient to convert from T_{mb} into T_{B} using formula (1). Number density of molecular gas toward the clumps WB89 673, WB89 668, S233-IR, G173.57+2.43, and S235-AB is within the range of $2.8\text{--}7.2 \times 10^3 \text{ cm}^{-3}$. The highest gas number density ($n = 7.2 \times 10^3 \text{ cm}^{-3}$) was detected toward the S233-IR. The kinetic tem-

Table 5. Clump sizes toward the star-forming regions S231–S235 from the data in the continuum at a wavelength of 1.1 mm from the Bolocam survey [26]. Root-mean-square deviation is given in brackets.

Source	θ_{maj} , ''	θ_{min} , ''
WB89 668	87 (12)	65 (10)
WB89 673	149 (13)	66 (5)
G173.57+2.43	81 (11)	59 (8)
S233-IR	67 (2)	53 (2)
S235 Central	163 (11)	96 (7)
S235 East1	125 (12)	55 (4)
S235 East2	93 (14)	86 (13)
S235-AB	86 (3)	65 (10)

perature for the clumps WB89 668, WB89 673 and G173.57+2.43 is nearly similar and equal to 14–16 K, and for S233-IR and S235-AB—27–30 K. The column density of ammonia N_{NH_3} is within the range of $2.2\text{--}12.4 \times 10^{14} \text{ cm}^{-2}$.

The brightest emission of ammonia was detected in S233-IR and WB89 673, and the gas temperature in these clumps is different: $T_{\text{kin}} = 29.4 \pm 11.8 \text{ K}$ and $T_{\text{kin}} = 15.9 \pm 1.5 \text{ K}$. It is notable that symmetric components of the hyperfine components in S233-IR have different intensities which is indicative of the effects of deviation from the LTE that we will discuss further.

6. DISCUSSION

Detection of all molecular clumps in the GMC G174+2.5 allows us to study conditions and sequence of star formation in it. The morphology of star-forming regions is complex, gas distribution is inhomogeneous which can be seen from Fig. 1. In the paper by Heyer et al. [22], they have concluded

Table 6. List of initial detection of molecular lines from the literature data and the results of this paper (marked with [tw]). Symbols + and – denoted the sources with and without the detected line respectively

Source	H ₂ O 22 GHz	NH ₃ 23 GHz	HC ₃ N 36 GHz	CH ₃ OH 36 GHz	SiO 86 GHz
WB89 690	+ [52]			+ [tw]	– [53]
WB89 668	+ [52]	+ [tw]	+ [tw]		
WB89 673	+ [52]	+ [tw]	+ [tw]	+ [tw]	+ [53]
G173.17+2.55		– [tw]			
G173.57+2.43	+ [52]	+ [54]			
S233-IR	+ [52]	+ [47]	+ [55]	+ [36]	+ [53]
S235 Central	+ [52]	+ [47]	+ [55]		– [53]
S235 East1	– [tw]	+ [13]			
S235 East2	– [tw]	+ [13]			+ [53]
S235-AB	+ [52]	+ [56]	+ [55]	+ [36]	– [53]

that there are molecular filaments connected with the regions S235 and S231. In the paper by Evans et al. [48], they say that there are two molecular clouds with different radial velocities around the H II S235 region. In the paper by Kirsanova et al. [12, 13], there is an interpretation of the kinematic structure of the S235 neighborhood within the model of triggered star formation scenario “collect-and-collapse” (see [49, 50]). In the paper by Ladeyshchikov et al. [51], it is shown that in the S233 region, expansion of the H II region has caused a collapse of a massive molecular clump initiating further star formation in it.

6.1. Dense Gas Distribution in the Regions S231–S235

In this paper, we show that spatial distribution of emission in the CO molecular lines can be used to study general characteristics of molecular clouds and to search for dense clumps with possible star formation in them. However, one single CO molecule is insufficient for the detailed study of star formation, as the emission in the CO molecule is indicative of the presence of medium-density gas and becomes saturated with higher density. In the case of an extended region of gas through the line of sight, its column density can be high from the CO-line estimations, however, the gas is not of high density actually. One of the most striking examples of such a situation can be observed in NGC 6334 [57], where the peak in the CO line does not correspond to the peaks in the HCO⁺, HCN and N₂H⁺ molecular lines. To prove the presence of high-density gas, additional observations in lines of molecules with high critical density are required. In the present paper, we use the lines of the HC₃N (4–3) and NH₃ (1,1) molecules, the critical densities of which are $n_{\text{crit}} \simeq 10^4 \text{ cm}^{-3}$ and $n_{\text{crit}} \simeq 10^3 \text{ cm}^{-3}$ respectively. Table 6 shows the lit-

erature data on the detection of lines-tracers of dense gas in the regions S231–S235. The HC₃N abundance is significant in dense heated gas near young stars (see, e.g., Meier et al. [58] and Lindberg et al. [59]), moreover, the HC₃N lines in star-forming regions are optically thin, as it was shown by Van den Bout [60].

The star-forming regions S231–S235 in the cyanoacetylene line were studied earlier in the paper by Alakoz et al. [61], but the emission at a level of $3\sigma = 0.25 \text{ K}$ was not detected for the sources S233-IR and S235-AB. In a year, however, the lines for three sources were detected in the paper by Pirogov et al. [55]. These sources were designated by the authors as S231, S235B, and S235 and associated with the molecular clumps S233-IR, S235-AB, and S235 Central respectively.

In accordance with the paper by Meier et al. [58], the cyanoacetylene emission is in good agreement with the emission in the continuum at 3 mm. According to the BGPS archive data [26], all the molecular clumps with the detected emission in the HC₃N line also radiate in the continuum at 1.2 mm. Nevertheless, we have not detected any emission toward S235 East1, S235 East2, and S235 Central, which can be associated with insufficient detection threshold of the observations.

For the first time, the ammonia line in S231–S235 was detected toward the source S235-AB almost at the same time by Ho et al. [62] and MacDonald et al. [56]. Later, Harju et al. [63] detected the ammonia line in the IRAS 05361+3539 source (our G173.57+2.43), Schreyer et al. [47]—in S233-IR, S235 Central, S235-AB, and Zinchenko et al. [46]—in the source S233-IR. Then in the paper by Kirsanova et al. [13], the region of S235 was studied in detail, also they obtained the maps of ammonia radio-brightness distribution and determined physical parameters of gas toward the following clusters: S235 East1, S235 East2, S235 Central, and S235-AB.

As seen from Fig. 4, the relation between the brightnesses of hyperfine components in S233-IR is irregular, i.e., it differs from the relation in the LTE conditions. In the paper by Stutzki et al. [64], it is shown that such an anomaly occurs when several small gas clumps fall into the beam of a telescope.

Virial stability in molecular clumps is described in detail in the paper by Kauffmann et al. [43]. It is usually supposed that if the virial parameter $\alpha_{\text{vir}} > \alpha_{\text{cr}}$, then a clump or a molecular cloud is gravitationally stable. If $\alpha_{\text{vir}} \lesssim \alpha_{\text{cr}}$, then density and pressure perturbation of a clump can cause a gravitational contraction of matter and starting star-formation processes. For isothermal clumps with the Jeans mass without considering magnetic fields— $\alpha_{\text{cr}} \simeq 2$ [43, 65]. As seen from Table 1, all the considered clumps $\alpha_{\text{vir}} \lesssim 2$, which is indicative of their gravitational instability.

Some molecular clumps in the CO line have a

complex extended structure that is not exactly described by the GaussClump algorithm, which supposes the Gaussian brightness distribution. The analysis shows that some molecular clumps divide into multiple components even with the use of a quite high threshold (1/7) for minimum source size. First of all, the clump G173.17+2.55 is referred to such clumps; it is a filament by structure and, thus, divides into the individual clumps NE and SW. Analogously, the molecular clump S235-Central is divided into two separate components (S235-Central E and S235-Central W), which agrees with the NH_3 emission structure from the paper by Kirsanova et al. [13]. To study the spatial-kinematic structure of such clumps, the observations of better resolution are required as well as applying of other methods of structure detection, such as GetFilaments [66], FIVE [67], and DisPerSe [68], etc.

6.2. Star Formation in Molecular Clumps

According to the modeling data from the paper by Clark et al. [69], the average column density of molecular clumps should exceed 10^{21} cm^{-2} to let star-formation processes start in them. Our paper shows that average gas column density in clumps from the data on the ^{13}CO emission is within the range of 1.4 to $4.3 \times 10^{22} \text{ cm}^{-2}$, thus, all the clumps under study are candidates star-forming regions.

Young star clusters in the GMC G174+2.5 were studied in the paper by Camargo et al. [20] using the photometry with the 2MASS data¹. They reported on 14 young star clusters embedded in molecular gas. Young star clusters toward the molecular clumps WB89 673 and WB89 668 have not been detected in their paper. All the clusters found are indicated with dashed circles in Fig. 1.

In accordance with [20], age, position, and sizes of young star clusters near S235 (S235 Central, East1, and East2) are in agreement with the scenario of the “collect-and-collapse” star formation process. Color characteristics of stars toward the molecular clumps S235-AB, S232-IR, S233-IR, and G173.57+2.43 match the characteristics of the embedded young star clusters. It is supposed that the age of these clusters is 3–5 Myr (see Table 2 from [20]) and they have not “scattered” the surrounding molecular gas yet.

Clusters in the S235-AB region were studied in the paper by Felli et al. [70–72]. They showed that the star cluster is located between the nebulae S235A and S235B, the first of which is an H II region. It is

shown in the paper by Boley et al. [73] that S235 B is a reflection nebula. They found a layer of heated molecular gas from the southern part of S235A. This gas is located between the H II region and the molecular cloud. In the more recent paper, Felli et al. [72] show that there are young stars in this layer. They deduced that the interaction of S235A and the surrounding molecular cloud probably caused the formation of the second generation of stars in this region.

Thus, young star clusters was detected toward all the considered molecular clumps except for G173.17+2.55, which are: S235 Central, S235 East1, S235 East2, S235-AB, S232-IR, S233-IR, G173.57+2.43, WB89 673, and WB89 668. The presence of young star clusters is indicative of active star-forming processes in the considered molecular clumps.

6.3. Evidence of Outflows in Molecular Clumps

In this Section, we will discuss the evidence of outflows in the studied massive clumps based on characteristics of maser emission of molecules.

Maser emission of methanol is a distinctive feature of star-forming regions. In the early studies of Batrla [74] and Menten [75], two types of methanol masers were distinguished empirically. Type II masers (e.g., at 6.7, 12, 37.7, and 107 GHz) pumped by IR emission of dust from young stars (see the papers by Sobolev et al. [76, 77]), thus, they are detected in the vicinity of such objects. Type I masers (e.g., at 36, 44, and 95 GHz) emerge as a result of collisional radiative pumping (see Sobolev et al. [5]) and usually indicate the presence of gas compressed by a shock wave. Such gas is often detected near young stars with an outflow interacting with ambient matter (see Voronkov et al. [9]). Emergence of molecular outflows from star-formation regions is an essential stage of star-formation process [78]. Type I masers are normally detected at some distance from young stellar objects, as is seen in the papers of Kurtz et al. [79], Voronkov et al. [9, 80]. However, type I methanol masers can arise in any region of the interstellar medium, where moderate-speed shock waves emerge: with the collisions of molecular clouds (see Salii et al. [8]), with the supernova explosions (see Pihlstrom et al. [81]), in places of interaction of H II regions and surrounding molecular gas (see Voronkov et al. [82]), and in the regions with complex hydrodynamic motions (see Voronkov et al. [83]).

In the methanol line at a frequency of 36.2 GHz, the emission toward S231–S235 was first detected in the paper by Haschick et al. [84], where they obtained the spectrum of the S235 source corresponding to the molecular clump S235-AB in the

¹ Two-Micron All-Sky Survey, available here www.ipac.caltech.edu/2mass/releases/allsky/

present paper. Later, in the paper by Liechti et al. [36], maser and thermal methanol lines were detected in two sources: S233-IR and S235-AB. In the methanol lines which we detected at 36 GHz in the sources WB89 673, S233-IR, and S235-AB, two components can be distinguished, wide and narrow. The wide component ($\geq 2.0 \text{ km s}^{-1}$) is often interpreted as “thermal” and the narrow component ($\leq 1.5 \text{ km s}^{-1}$)—as “maser” [36]. According to the conclusions by Berulis et al. [33], the “maser” component can originate both in protostar neighborhood and in a usual gravitationally stable fragment of the interstellar medium emerging due to turbulence. Type I methanol masers can also be associated with protostars at the early stages of collapse (see Sobolev et al. [85], Sutton et al. [7]) and form at the borders of hypercompact H II regions (see Sobolev et al. [5]). Thus, a methanol maser can not be a definitive criterion of the presence of outflows from young stellar objects at early star-forming stages.

It should be noted that there is a restriction to methanol formation in shock waves. In accordance with the paper by Garay et al. [86], methanol can not exist in shock waves moving with speeds exceeding 10 km s^{-1} , as these molecules decay at high speeds. As an additional indicator of shock waves associated with outflows from young stellar objects, one can use the SiO molecular lines, see the papers by Schilke et al. [87] and Caselli et al. [88]. With the shock wave propagation, the methanol abundance of the gas phase increases owing to evaporation from the dust-particle surface [8]. Compared to methanol, the SiO molecule does not decay at high speeds of shock waves (from 10 to 40 km s^{-1} , see [87]), thus, emission in the SiO lines is a reliable tracer of outflows. The existence of outflows from the young molecular clumps WB89 673 and S233-IR is proved by the presence of the SiO outflow in the paper by Harju et al. [53]. The outflow in S233-IR has been studied earlier in the literature (see [15, 89–91]), where they show that it emerges in the massive-star forming region. The SiO emission in S235-AB was not detected in [53], although, there is the emission observed in the maser methanol lines in this clump at 36 GHz [36, 84].

In most cases, the maser emission of water is detected in star-forming regions (see Section 6.1.1 from Gray [10]). The presence of water masers toward the molecular clumps in the S231–S235 regions is additional evidence of active star-formation processes ongoing in them. The H₂O masers were detected toward the clumps WB89 690, WB89 668, WB89 673, G173.57+2.43, S233-IR, S235 Central, and S235-AB (see Table 6).

The outflow in the S235-AB region was proved in a series of papers by Felli et al. [70–72]. It is shown in the paper by Shepherd and Watson [19] that at least two young stellar objects from the cluster are

responsible for matter outflow in the G173.58+2.43 region.

Thus, molecular outflow evidence are found in the following massive clumps: WB89 690, WB89 668, WB89 673, G173.57+2.43, S233-IR, S235 Central, S235 East2, and S235-AB. They are not found toward S235 East1 and G173.17+2.55.

7. CONCLUSION

(1) Based on the archive data on the CO molecule, we identified 10 massive star-forming clumps in the giant molecular cloud G174+2.5. All of them belong to the star-forming regions S231–S235 which took their names from the H II regions located in them.

(2) The clumps are gravitationally unstable and, from the CO data, their masses are within the range of about 700 to $2000 M_{\odot}$.

(3) As a result of observations, we obtained the spectra of the methanol, cyanoacetylene, and ammonia lines:

- The emission in the cyanoacetylene line at 36.4 HGz was detected toward three molecular clumps: WB89 668, WB89 673, and S233-IR. It indicates high density of molecular gas. The HC₃N column density appear to be sufficient for being detected on the RT-22 radio telescope.
- The methanol line at 36.2 HGz was detected toward WB89 673, S233-IR, and S235-AB. Detection of emission in this line denotes the shock fronts in the clumps.
- The emission in the ammonia line was detected toward 6 clumps: WB89 668, WB89 673, S233-IR, G173.57+2.43, S235 AB, and S235 Central. Physical parameters of the molecular clumps were determined from the ammonia line: temperature, column density of ammonia, and molecular gas number density. It was determined that the clump temperature is within the range of 16 to 30 K and the molecular gas number density—of 2800 to 7200 cm^{-3} .

(4) Embedded young stellar clusters are found in all the clumps except for G173.17+2.55.

(5) Molecular outflow evidence are observed toward all massive clumps except for S235 East1 and G173.17+2.55.

ACKNOWLEDGMENTS

The study was supported with the program 211 of the Government of the Russian Federation, agreement №02.A03.21.0006. The work was partially supported by the Ministry of Education and Science of the Russian Federation (state assignment №3.1781.2014/K).

D. A. Ladeyshchikov is thankful to G. T. Smirnov, V. A. Gusev, and S. V. Logvinenko for guidance,

support, and help in development of the automation system for the RT-22 double-channel radiometer.

M. S. Kirsanova is grateful to the Russian Science Foundation (grant MK-2570.2014.2) and the PSD-15 program of the Physical Sciences Department of the Russian Academy of Sciences.

A. P. Tsivilev thanks the PSD program “Interstellar and Intergalactic Medium: Active and Extended Objects”.

-
1. F. Combes, *Annu. Rev. Astron. Astrophys.* **29**, 195 (1991).
 2. C. M. Walmsley and H. Ungerechts, *Astron. Astrophys.* **122**, 164 (1983).
 3. J. Jijina, P. C. Myers, and F. C. Adams, *Astrophys. J., Suppl. Ser.* **125**, 161 (1999).
 4. M. Morris, B. E. Turner, P. Palmer, and B. Zuckerman, *Astrophys. J.* **205**, 82 (1976).
 5. A. M. Sobolev, D. M. Cragg, S. P. Ellingsen, et al., in *IAU Symposium*, Edited by J. M. Chapman and W. A. Baan (Cambridge University Press, New York, 2007), *IAU Symposium*, vol. 242, pp. 81–88.
 6. S. V. Salii and A. M. Sobolev, *Astron. Rep.* **50**, 965 (2006).
 7. E. C. Sutton, A. M. Sobolev, S. V. Salii, et al., *Astrophys. J.* **609**, 231 (2004).
 8. S. V. Salii, A. M. Sobolev, and N. D. Kalinina, *Astron. Rep.* **46**, 955 (2002).
 9. M. A. Voronkov, K. J. Brooks, A. M. Sobolev, et al., *Mon. Not. R. Astron. Soc.* **373**, 411 (2006).
 10. M. Gray, *Maser Sources in Astrophysics* (Cambridge University Press, New York, 2012).
 11. S. Sharpless, *Astrophys. J., Suppl. Ser.* **4**, 257 (1959).
 12. M. S. Kirsanova, A. M. Sobolev, M. Thomasson, et al., *Mon. Not. R. Astron. Soc.* **388**, 729 (2008).
 13. M. S. Kirsanova, D. S. Wiebe, A. M. Sobolev, et al., *Mon. Not. R. Astron. Soc.* **437**, 1593 (2014).
 14. L. Chavarría, L. Allen, C. Brunt, et al., *Mon. Not. R. Astron. Soc.* **439**, 3719 (2014).
 15. A. G. Ginsburg, J. Bally, C.-H. Yan, and J. P. Williams, *Astrophys. J.* **707**, 310 (2009).
 16. S. Leurini, H. Beuther, P. Schilke, et al., *Astron. Astrophys.* **475**, 925 (2007).
 17. H. Beuther, S. Leurini, P. Schilke, et al., *Astron. Astrophys.* **466**, 1065 (2007).
 18. A. Chakraborty, D. K. Ojha, B. G. Anandarao, and T. N. Rengarajan, *Astron. Astrophys.* **364**, 683 (2000).
 19. D. S. Shepherd and A. M. Watson, *Astrophys. J.* **566**, 966 (2002).
 20. D. Camargo, C. Bonatto, and E. Bica, *Mon. Not. R. Astron. Soc.* **416**, 1522 (2011).
 21. J. G. A. Wouterloot and J. Brand, *Astron. Astrophys., Suppl. Ser.* **80**, 149 (1989).
 22. M. H. Heyer, J. M. Carpenter, and E. F. Ladd, *Astrophys. J.* **463**, 630 (1996).
 23. R. A. Burns, H. Imai, T. Handa, et al., *Mon. Not. R. Astron. Soc.* **453**, 3163 (2015).
 24. B. Reipurth and C.-H. Yan, *Star Formation and Molecular Clouds towards the Galactic Anti-Center* (Astronomical Society of the Pacific, San Francisco, 2008).
 25. T. M. Dame, D. Hartmann, and P. Thaddeus, *Astrophys. J.* **547**, 792 (2001).
 26. A. Ginsburg, J. Glenn, E. Rosolowsky, et al., *Astrophys. J., Suppl. Ser.* **208**, 14 (2013).
 27. E. L. Wright, P. R. M. Eisenhardt, A. K. Mainzer, et al., *Astron. J.* **140**, 1868 (2010).
 28. A. Lawrence, S. J. Warren, O. Almaini, et al., *Mon. Not. R. Astron. Soc.* **379**, 1599 (2007).
 29. J. C. Mottram, C. M. Brunt, and M. H. Heyer, “High Resolution Multi-Isotopic Maps of CO Integrated Intensity in the Galactic Plane,” .
 30. R. J. Sault, P. J. Teuben, and M. C. H. Wright, in *Astronomical Data Analysis Software and Systems IV*, Edited by R. A. Shaw, H. E. Payne, and J. J. E. Hayes (1995), *Astronomical Society of the Pacific Conference Series*, vol. 77, p. 433.
 31. W. A. Joye and E. Mandel, in *Astronomical Data Analysis Software and Systems XII*, Edited by H. E. Payne, R. I. Jedrzejewski, and R. N. Hook (Astronomical Society of the Pacific, San Francisco, 2003), *Astronomical Society of the Pacific Conference Series*, vol. 295, p. 489.
 32. A. M. Tolmachev and R. L. Sorochenko, *Sov. Astron. Lett* **7**, 379 (1981).
 33. I. I. Berulis, S. V. Kalenski, A. M. Sobolev, and V. S. Streinitski, *Astron. Astrophys. Trans.* **1**, 231 (1992).
 34. T. L. Wilson and R. Mauersberger, *Astron. Astrophys.* **239**, 305 (1990).
 35. I. I. Berulis, V. A. Gusev, A. V. Kutsenko, et al., *Tr. Akad. Nauk SSSR Phys. Inst.* **135**, 35 (1983).
 36. S. Liechti and T. L. Wilson, *Astron. Astrophys.* **314**, 615 (1996).
 37. S. Maret, P. Hily-Blant, J. Pety, et al., *Astron. Astrophys.* **526**, A47 (2011).
 38. J. Roman-Duval, J. M. Jackson, M. Heyer, et al., *Astrophys. J.* **723**, 492 (2010).
 39. R. Simon, J. M. Jackson, D. P. Clemens, et al., *Astrophys. J.* **551**, 747 (2001).
 40. M. J. Reid, *Annu. Rev. Astron. Astrophys.* **31**, 345 (1993).
 41. W. D. Langer and A. A. Penzias, *Astrophys. J.* **357**, 477 (1990).
 42. J. Stutzki and R. Guesten, *Astrophys. J.* **356**, 513 (1990).

43. J. Kauffmann, T. Pillai, and P. F. Goldsmith, *Astrophys. J.* **779**, 185 (2013).
44. P. Padoan, M. Juvela, J. Bally, and Å. Nordlund, *Astrophys. J.* **529**, 259 (2000).
45. K. Rohlfs and T. L. Wilson, *Tools of radio astronomy* (Springer, New York).
46. I. Zinchenko, T. Henning, and K. Schreyer, *Astron. Astrophys.*, Suppl. Ser. **124**, 385 (1997).
47. K. Schreyer, T. Henning, C. Koempe, and P. Harjunpää, *Astron. Astrophys.* **306**, 267 (1996).
48. N. J. Evans, II and G. N. Blair, *Astrophys. J.* **246**, 394 (1981).
49. B. G. Elmegreen and C. J. Lada, *Astrophys. J.* **214**, 725 (1977).
50. A. P. Whitworth, A. S. Bhattal, S. J. Chapman, et al., *Mon. Not. R. Astron. Soc.* **268**, 291 (1994).
51. D. A. Ladeyschkov, A. M. Sobolev, M. Thomasson, et al., *Mon. Not. R. Astron. Soc.* **452**, 2306 (2015).
52. J. G. A. Wouterloot, J. Brand, and K. Fiegle, *Astron. Astrophys.*, Suppl. Ser. **98**, 589 (1993).
53. J. Harju, K. Lehtinen, R. S. Booth, and I. Zinchenko, *Astron. Astrophys.*, Suppl. Ser. **132**, 211 (1998).
54. J. G. A. Wouterloot, C. M. Walmsley, and C. Henkel, *Astron. Astrophys.* **203**, 367 (1988).
55. L. E. Pirogov, L. E. B. Johansson, and I. I. Zinchenko, *Astron. Astrophys. Trans.* **22**, 33 (2003).
56. G. H. MacDonald, L. T. Little, A. T. Brown, et al., *Mon. Not. R. Astron. Soc.* **195**, 387 (1981).
57. A. J. Walsh, S. Thorwirth, H. Beuther, and M. G. Burton, *Mon. Not. R. Astron. Soc.* **404**, 1396 (2010).
58. D. S. Meier and J. L. Turner, *Astrophys. J.* **618**, 259 (2005).
59. J. E. Lindberg, S. Aalto, F. Costagliola, et al., *Astron. Astrophys.* **527**, A150 (2011).
60. P. A. Vanden Bout, R. B. Loren, R. L. Snell, and A. Wootten, *Astrophys. J.* **271**, 161 (1983).
61. A. V. Alakoz, S. V. Kalenskii, V. G. Promislov, et al., *Astron. Rep.* **46**, 551 (2002).
62. P. T. P. Ho, R. N. Martin, and A. H. Barrett, *Astrophys. J.* **246**, 761 (1981).
63. J. Harju, M. Walmsley, and J. G. A. Wouterloot, in *Fragmentation of Molecular Clouds and Star Formation*, Edited by E. Falgarone, F. Boulanger, and G. Duvert (Kluwer Academic Publishers, Dordrecht, 1991), *IAU Symposium*, vol. 147, p. 436.
64. J. Stutzki and G. Winnewisser, *Astron. Astrophys.* **144**, 13 (1985).
65. C. F. McKee and E. G. Zweibel, *Astrophys. J.* **399**, 551 (1992).
66. A. Men'shchikov, *Astron. Astrophys.* **560**, A63 (2013).
67. A. Hacar, M. Tafalla, J. Kauffmann, and A. Kovács, *Astron. Astrophys.* **554**, A55 (2013).
68. T. Sousbie, *Mon. Not. R. Astron. Soc.* **414**, 350 (2011).
69. P. C. Clark and S. C. O. Glover, *Mon. Not. R. Astron. Soc.* **444**, 2396 (2014).
70. M. Felli, L. Testi, R. Valdettaro, and J.-J. Wang, *Astron. Astrophys.* **320**, 594 (1997).
71. M. Felli, F. Massi, A. Navarrini, et al., *Astron. Astrophys.* **420**, 553 (2004).
72. M. Felli, F. Massi, M. Robberto, and R. Cesaroni, *Astron. Astrophys.* **453**, 911 (2006).
73. P. A. Boley, A. M. Sobolev, V. V. Krushinsky, et al., *Mon. Not. R. Astron. Soc.* **399**, 778 (2009).
74. W. Batrla, H. E. Matthews, K. M. Menten, and C. M. Walmsley, *Nature* **326**, 49 (1987).
75. K. M. Menten, *Astrophys. J.* **380**, L75 (1991).
76. A. M. Sobolev, A. B. Ostrovskii, M. S. Kirsanova, et al., in *Massive Star Birth: A Crossroads of Astrophysics*, Edited by R. Cesaroni, M. Felli, E. Churchwell, and M. Walmsley (Cambridge University Press, New York, 2005), *IAU Symposium*, vol. 227, pp. 174–179.
77. D. M. Cragg, A. M. Sobolev, and P. D. Godfrey, *Mon. Not. R. Astron. Soc.* **360**, 533 (2005).
78. R. Bachiller, *Annu. Rev. Astron. Astrophys.* **34**, 111 (1996).
79. S. Kurtz, P. Hofner, and C. V. Álvarez, *Astrophys. J.*, Suppl. Ser. **155**, 149 (2004).
80. M. A. Voronkov, J. L. Caswell, S. P. Ellingsen, et al., *Mon. Not. R. Astron. Soc.* **439**, 2584 (2014).
81. Y. M. Pihlström, L. O. Sjouwerman, D. A. Frail, et al., *Astron. J.* **147**, 73 (2014).
82. M. A. Voronkov, J. L. Caswell, S. P. Ellingsen, and A. M. Sobolev, *Mon. Not. R. Astron. Soc.* **405**, 2471 (2010).
83. M. A. Voronkov, J. L. Caswell, T. R. Britton, et al., *Mon. Not. R. Astron. Soc.* **408**, 133 (2010).
84. A. D. Haschick and W. A. Baan, *Astrophys. J.* **339**, 949 (1989).
85. A. M. Sobolev and V. S. Strel'nitskij, *Pisma Astron. Zh.* **9**, 26 (1983).
86. G. Garay, D. Mardones, L. F. Rodríguez, et al., *Astrophys. J.* **567**, 980 (2002).
87. P. Schilke, C. M. Walmsley, G. Pineau des Forets, and D. R. Flower, *Astron. Astrophys.* **321**, 293 (1997).
88. P. Caselli, T. W. Hartquist, and O. Havnes, *Astron. Astrophys.* **322**, 296 (1997).
89. A. Porras, I. Cruz-González, and L. Salas, *Astron. Astrophys.* **361**, 660 (2000).
90. H. Beuther, P. Schilke, F. Gueth, et al., *Astron. Astrophys.* **387**, 931 (2002).
91. T. Khanzadyan, M. D. Smith, C. J. Davis, and T. Stanke, *Astron. Astrophys.* **418**, 163 (2004).
92. G. A. Blake, E. C. Sutton, C. R. Masson, and T. G. Phillips, *Astrophys. J.* **315**, 621 (1987).
93. R. H. Hildebrand, *Quart. J. R. Astron. Soc.* **24**, 267 (1983).
94. P. T. P. Ho and C. H. Townes, *Annu. Rev. Astron. Astrophys.* **21**, 239 (1983).
95. J. G. Mangum, A. Wootten, and L. G. Mundy, *Astrophys. J.* **388**, 467 (1992).
96. G. Danby, D. R. Flower, P. Valiron, et al., *Mon. Not. R. Astron. Soc.* **235**, 229 (1988).

APPENDIX A: A. ESTIMATION OF MOLECULAR CLOUD MASSES FROM THE CO RADIO LINES

The presented method is intended to determine physical parameters of molecular clouds from the data in the CO lines. In general, the method corre-

sponds to the one in the paper by Roman-Duval et al. [38] with some changes concerning the detection of column densities and clump masses. To estimate the column density, we used the LTE assumption. It was also supposed that the ^{12}CO lines are optically thick. In this case, the excitation temperature T_{ex} of the line can be determined from the radiative transfer equation (formula 15.29 from [45]) for the $^{12}\text{CO}(1-0)$ line:

$$T_{\text{ex}} = 5.53 / \ln \left(1 + \frac{5.53}{T_{\text{B}}^{12} + 0.837} \right) \quad (\text{A1})$$

where T_{B}^{12} —the brightness temperature of the $^{12}\text{CO}(1-0)$ line. In the present case, the microwave background $T_{\text{bg}} = 2.7$ K is taken into account. As the average size of sources in the ^{12}CO and ^{13}CO (from 1'.9 to 4'.1, see Table 1) is bigger than the beam width (45''), $T_{\text{B}} = T_{\text{mb}}$.

To determine the optical depth and CO column density, we used the isotope of the ^{13}CO molecule, as it is less abundant, and its optical depth is smaller as compared to ^{12}CO . The latter results in the fact that emission is less subject to saturation effects. The optical depth of the $^{13}\text{CO}(1-0)$ line can be derived with formula (15.31) from [45]:

$$\tau_0^{13} = -\ln \left[1 - \frac{T_{\text{B}}^{13}}{5.3} \left\{ \left[\exp \left(\frac{5.3}{T_{\text{ex}}} \right) - 1 \right]^{-1} - 0.16 \right\} \right], \quad (\text{A2})$$

where T_{B}^{13} —the brightness temperature of the $^{13}\text{CO}(1-0)$ line, T_{ex} —the excitation temperature. For the CO linear molecule, the excitation is characterized by the same temperature T_{ex} , thus, the column density N and optical depth τ are connected with the following relation (see equation 3 from [38]):

$$N(^{13}\text{CO}) = 2.6 \times 10^{14} \frac{T_{\text{ex}}}{1 - \exp(-5.3/T_{\text{ex}})} \times \int \tau^{13}(v) dv, \quad (\text{A3})$$

moreover, in the case of the Gaussian profile of optical depth $\int \tau^{13}(v) dv = \tau_0^{13} \sigma_v \sqrt{2\pi}$, where σ_v is the ^{13}CO line velocity dispersion, τ_0 is the optical depth in the center of the line. The H_2 column density is derived from the abundances of $^{12}\text{CO}/^{13}\text{CO}$ and also CO/H_2 :

$$N(\text{H}_2) = N(^{13}\text{CO}) \times \frac{^{12}\text{CO}}{^{13}\text{CO}} \left[\frac{\text{CO}}{\text{H}_2} \right]^{-1} \quad (\text{A4})$$

The relation $\text{CO}/\text{H}_2 \simeq 8 \times 10^{-5}$ is in accordance with [92]. The relation $^{12}\text{CO}/^{13}\text{CO}$ varies from 40

to 70 depending on the distance from the Galactic center to the source according to [41]. At a distance of 2 kpc from the Sun in the direction to the galactic anticenter, the ratio of abundances is $^{12}\text{CO}/^{13}\text{CO} \simeq 70$.

The mass is determined as a integration of column density distribution $N(\text{H}_2)$ on the source surface dA :

$$M = \mu m_{\text{H}_2} \int N_{\text{H}_2} dA = \mu m_{\text{H}_2} D^2 \int N_{\text{H}_2} d\Omega, \quad (\text{A5})$$

where μ is the ratio of the interstellar gas to the mass of the hydrogen molecule, $\mu \approx 1.33$ [93], m_{H_2} is the mass of the hydrogen molecule and the surface element is dA related with the solid angle through the relation $dA = D^2 d\Omega$, where D is the distance to the source in kpc.

When combining expressions (A4) and (A5) and insertion of numerical constants, we obtain the following expression for the source mass:

$$M = 0.41 D^2 \int_{\alpha, \delta} \frac{T_{\text{ex}} \tau^{13} \sigma_v \sqrt{2\pi}}{1 - \exp(-5.3/T_{\text{ex}})} \Delta\alpha \Delta\delta \quad (M_{\odot}) \quad (\text{A6})$$

where $T_{\text{ex}} = T_{\text{ex}}(\alpha, \delta)$ is the excitation temperature in the given map cell which is calculated with formula (A1), $\tau^{13} = \tau^{13}(\alpha, \delta)$ is the optical depth of ^{13}CO in the center of the line profile of the given map cell which is calculated with formula (A2), $\sigma_v = \sigma_v(\alpha, \delta)$ is the ^{13}CO line-profile velocity dispersion, $\Delta\alpha$ and $\Delta\delta$ is the size of a map cell along α and δ expressed in arcminutes. A coefficient preceding the integral, 0.41, differs from the value 0.27 accepted in the paper by Roman-Duval et al. [38] due to using a different ratio of abundances $^{12}\text{CO}/^{13}\text{CO}$ (70 instead of 45).

The virial parameter of the clumps $\alpha_{\text{vir}} \equiv M_{\text{vir}}/M$ is calculated in accordance with the definition given in [43]:

$$\alpha_{\text{vir}} = \frac{5\sigma_v^2 R}{GM} = 1.2 \left(\frac{\sigma_v}{\text{km s}^{-1}} \right)^2 \left(\frac{R}{\text{pc}} \right) \left(\frac{M}{M_{\odot}} \right)^{-1} \quad (\text{A7})$$

The clump radii are derived as in [38] from the area which is occupied by a clump at the full width of half maximum:

$$R = \sqrt{\frac{A}{\pi}} = \sqrt{\frac{\Omega D^2}{\pi}} = \sqrt{\frac{N_{\text{pix}} \Delta\alpha \Delta\delta D^2}{\pi}}, \quad (\text{A8})$$

where N_{pix} is the number of map cells occupied by a clump, $\Delta\alpha$ and $\Delta\delta$ are the map cell sizes. The velocity dispersion σ_v in the ^{13}CO molecular line is calculated with the formula according to [38]:

$$\sigma_v^2 = \frac{\sum T_{13}(v - \bar{v})^2}{\sum T_{13}}, \quad (\text{A9})$$

and addition in formula (A9) is done along (α, δ, v) for those T_{13} values that exceed the intensity level 4σ .

APPENDIX B: B. METHOD OF ESTIMATION
OF MOLECULAR GAS PHYSICAL
PARAMETERS FROM THE AMMONIA RADIO
LINES

The emission spectrum of the ammonia line is described in detail in [94]. Here we present the end formulae only which we have used when estimating the gas temperature, its density, and ammonia abundance in it. It is known that populations of metastable levels (1,1) and (2,2) are determined by collisions which allows us to use the assumption on the LTE and estimate the kinetic gas temperature T_{gas} . Using the NH3(1,1) method from the CLASS package, one can estimate the optical depth of the main component $\tau_{(1,1)\text{m}}$. Further, the excitation temperature of transition (1,1) is determined which is supposed to be similar for all other inversion transitions in the LTE conditions:

$$T_{\text{ex}} = \frac{T_{\text{B}(1,1)}}{1 - \exp(-\tau_{(1,1)\text{m}})} + T_{\text{bg}} \quad (\text{K}), \quad (\text{B1})$$

Table 4 shows the brightness temperature of the main component of (1,1) line, $T_{\text{B}(1,1)}$. The T_{bg} value is the background temperature which is determined by the temperature of the cosmological microwave background and the background emission of a source T_{s} :

$$T_{\text{bg}} = 2.73 + T_{\text{s}} \quad (\text{K}). \quad (\text{B2})$$

The column density of ammonia at level (1,1) is estimated as in [95]:

$$N_{(1,1)} = 6.60 \times 10^{14} \frac{T_{\text{ex}}}{\nu_{(1,1)}} \tau_{(1,1)\text{m}} \times \Delta V_{(1,1)} \quad (\text{cm}^{-2}), \quad (\text{B3})$$

where $\Delta V_{(1,1)}$ is the (1,1) line width in km s^{-1} , its value is given in Table 4, $\nu_{(1,1)} = 23.7$ is the transition (1,1) frequency in GHz.

The total column density of ammonia in the LTE conditions in terms of four low levels: the ground one and (1,1), (2,2), and (3,3) is equal to:

$$N_{\text{NH}_3} = N_{(1,1)} \left(\frac{1}{3} e^{\frac{21.3}{T_{\text{rot}}}} + 1 + \frac{5}{3} e^{\frac{-41.2}{T_{\text{rot}}}} + \frac{14}{3} e^{\frac{-99.4}{T_{\text{rot}}}} \right) \quad (\text{cm}^{-2}), \quad (\text{B4})$$

where T_{rot} is the rotational temperature determining the relation of populations between levels (2,2) and (1,1).

In the LTE conditions [94]:

$$T_{\text{rot}} = -41.5 \ln \left(\frac{-0.282}{\tau_{(1,1)\text{m}}} \ln \left(1 - \frac{T_{\text{B}(2,2)\text{m}}}{T_{\text{B}(1,1)\text{m}}} \times (1 - e^{-\tau_{(1,1)\text{m}}}) \right) \right)^{-1} \quad (\text{K}). \quad (\text{B5})$$

To estimate T_{gas} , one uses the relation obtained in [2] with the coefficients from [96]:

$$T_{\text{rot}} = \frac{T_{\text{gas}}}{1 + \frac{T_{\text{gas}}}{41.5} \ln \left(1 + \frac{C_{(2,2 \rightarrow 2,1)}}{C_{(2,2 \rightarrow 1,1)}} \right)} \quad (\text{K}), \quad (\text{B6})$$

The coefficients $C_{(2,2 \rightarrow 2,1)}$ and $C_{(2,2 \rightarrow 1,1)}$ are given in a tabulated form in [96] for several T_{gas} values. Equation (B6) can be solved with the iteration method.

If we know T_{ex} , we can estimate the molecular gas number density $n(\text{H}_2)$ taking into consideration only two levels of inversion transition (1,1) with the use of the following relation [94]:

$$n(\text{H}_2) = \frac{A_{(1,1)}}{C_{(1,1)}} \left(\frac{J_{\nu}(T_{\text{ex}}) - J_{\nu}(T_{\text{bg}})}{J_{\nu}(T_{\text{gas}}) - J_{\nu}(T_{\text{ex}})} \right) \times \left(1 + \frac{J_{\nu}(T_{\text{gas}})}{h\nu_{(1,1)}/k} \right) \quad (\text{cm}^{-3}), \quad (\text{B7})$$

where

$$J_{\nu}(T) = \frac{h\nu_{(1,1)}}{k} \left(\exp \frac{h\nu_{(1,1)}}{kT} - 1 \right). \quad (\text{B8})$$

The coefficient $A_{(1,1)} = 1.7 \times 10^{-7} \text{ s}^{-1}$ [45], and $C_{(1,1)}$ is taken from Table in [96] for the certain T_{gas} value.